Journal of Alloys and Compounds 509 (2011) 10115–10120

Contents lists available at ScienceDirect

Journal of Alloys and Compounds

journal homepage: www.elsevier.com/locate/jallcom

Luminescent properties and X-ray photoelectron spectroscopy study of $ZnAl_2O_4$:Ce^{3+},Tb^{3+} phosphor

K.G. Tshabalala[a], S.-H. Cho[b], J.-K. Park[b], Shreyas S. Pitale[a], I.M. Nagpure[a], R.E. Kroon[a], H.C. Swart[a], O.M. Ntwaeaborwa[a,*]

[a] Department of Physics, University of the Free State, Bloemfontein, ZA9300, South Africa
[b] Nano-Materials Center, Korea Institute of Science and Technology, Cheongryang, 39-1 Hawolkok, Seoul 136-791, South Korea

ARTICLE INFO

Article history:
Received 14 March 2011
Received in revised form 9 August 2011
Accepted 10 August 2011
Available online 19 August 2011

Keywords:
Spinel
Crystallite size
Photoluminescence
Excitation

ABSTRACT

Cerium (Ce^{3+})- and terbium (Tb^{3+}) co-doped zinc aluminate ($ZnAl_2O_4$) nanocrystals were successfully prepared by a combustion method using urea as fuel. The as-prepared samples were annealed in hydrogen atmosphere to improve their optical properties and crystallinity. The structure and morphology of the samples analyzed using X-ray diffraction (XRD) and high resolution transmission electron microscopy (HRTEM) showed that $ZnAl_2O_4$ crystallized in a well known cubic spinel structure. As deduced from X-ray photoelectron spectroscopy (XPS) data, there was partial inversion of cations in as-prepared (unannealed) samples implying that the $ZnAl_2O_4$ did not crystallize in a cubic normal spinel. Instead, the XPS data demonstrated possible structural readjustment from inverse to normal spinel after annealing. The excitation and emission data collected when $ZnAl_2O_4$:Ce^{3+},Tb^{3+} samples, with different concentrations of Ce^{3+} and Tb^{3+} ions, were excited at different wavelengths showed that green emission of Tb^{3+} was sensitized by Ce^{3+}, i.e. there was energy transfer from Ce^{3+} to Tb^{3+} resulting in improvement of green emission from Tb^{3+}. This study therefore, sets out to discuss the sensitizing effect of Ce^{3+} and the effect of annealing on the structure of $ZnAl_2O_4$:Ce^{3+},Tb^{3+}.

1. Introduction

Zinc aluminate ($ZnAl_2O_4$) is a well known semiconductor with a wide bulk band gap of 3.5–3.9 eV [1–6]. It belongs to a class of mixed-metal oxides called the spinels which are commonly represented by a general chemical formula AB_2O_4 where A and B are divalent (2+) and trivalent (3+) cations, respectively. In AB_2O_4 spinels, 8 of the 64 tetrahedral interstices are occupied by A^{2+} cations while 16 of the 32 octahedral interstices are occupied by B^{3+} cations [7]. It is well known that $ZnAl_2O_4$ can crystallize in a cubic normal or inverse spinel structure depending on the preparation procedure. In the normal spinel structure, the 3+ ions occupy the octahedral site while the 2+ ions occupy the tetrahedral site. In an inverse spinel the divalent and trivalent ions are not just exchanged but there is a mixed occupation by different amounts of A^{2+} and B^{3+} on the octahedral site while the tetrahedral site is only occupied by the B^{3+} cations. In most cases, intermediate structures between normal and inverse spinels are crystallized [8]. Traditionally, $ZnAl_2O_4$ with normal, intermediate or inverse spinel structure is widely used as a catalyst or ceramic [9]. Today, it is used in many applications such as optoelectronics, sensor technology and information display technology [1,2,5,6] because of its excellent optical and hydrophobic properties and high chemical and thermal stability [10]. For application in display technologies, $ZnAl_2O_4$ is used as host matrix for trivalent rare-earth ions (e.g. Tb^{3+}, Eu^{3+} and Dy^{3+}) [11–13] or transition metals (e.g. Mn^{2+} and Cr^{3+}) [14,15] to prepare phosphors emitting mostly in the visible range of the electromagnetic spectrum. Researchers in this study are particularly interested in the performance of a nanocrystalline $ZnAl_2O_4$ because of the speculation that nanocrystalline materials may have better optical properties than their bulk counterparts [11]. Different synthesis methods such as sol–gel [16,17], hydrothermal [18,19], combustion [6,15,20] and solid state reaction [21] are commonly used to prepare rare-earth/transition metal doped nanocrystalline $ZnAl_2O_4$ phosphors. In this study, the solution combustion method was used to prepare Ce^{3+}–Tb^{3+} co-activated nanocrystalline $ZnAl_2O_4$ phosphors. Compared to other methods, the combustion method has advantages such as cost-effectiveness, low processing temperature, extremely shorter reaction time, high purity and homogeneity of the final product. The flame temperature during urea assisted combustion was sufficient to enable some Al ions in the zinc aluminate spinel structure to occupy tetrahedral sites (spinel inversion) [22]. The objective of this study was to prepare an efficient green emitting phosphor through sensitization of Tb^{3+} by Ce^{3+}. It is well known that Ce^{3+} can absorb UV photons and sensitize emission of

* Corresponding author. Tel.: +27 51 401 2193; fax: +27 51 401 3507.
E-mail addresses: tshabalalakg@ufs.ac.za (K.G. Tshabalala), ntwaeab@ufs.ac.za (O.M. Ntwaeaborwa).

0925-8388/$ – see front matter © 2011 Elsevier B.V. All rights reserved.
doi:10.1016/j.jallcom.2011.08.054

other rare-earth by a down-conversion process [23,24]. This study was also intended to investigate the effects of different parameters such as relatively low activator concentrations, annealing temperature and excitation wavelengths on emission efficiency of nanocrystalline $ZnAl_2O_4$:Ce,Tb phosphor. In addition, the X-ray photoelectron spectroscopy (XPS) was used to determine the chemical and electronic states of the elements present in as prepared and post-preparation annealed samples. This phosphor was evaluated for application in display technologies and also as a UV down-converting layer for improved efficiency of photovoltaic cells.

2. Experimental details

2.1. Powder preparation

The raw materials used were analytical reagent (AR) grade zinc nitrate hexahydrate, aluminum nitrate, rare-earth nitrates (cerium nitrate and terbium nitrate), and urea (ACS reagent). All these were of AR grade from Merck South Africa with ~99% purity, while the rare-earth (Ce^{3+} and Tb^{3+}) nitrates with ~99.99% purity were from Aldrich–Sigma. Stochiometric amounts of zinc nitrate, aluminum nitrate and urea were dissolved in triple de-ionized (DI) water. A homogeneous transparent solution was obtained after stirring vigorously for 20 min. The solution was transferred to a muffle furnace maintained at 400 ± 10 °C. After all the liquid had evaporated, the mixture decomposed and released large amount of gases. Due to the exothermic nature of this process, the reaction continued for a while and the mixture swelled to a larger volume. Large exothermicity resulted in a flame that further decomposed the mixture into gaseous phases and aluminates. The flame persisted for ~45 s. The entire combustion process was completed in less than 5 min. The powder products were gently ground using an alumina mortar and pestle and were then annealed at different temperatures either in air or hydrogen atmosphere to improve their crystallinity and optical properties. $ZnAl_2O_4$:Ce^{3+},Tb^{3+} powder phosphors with different concentrations of Ce^{3+} and Tb^{3+} were prepared and investigated. The amounts of zinc nitrate, aluminum nitrate and urea used were 2.91 g, 7.57 g and 4.037 g, respectively. To avoid concentration quenching effects, the dopants (Ce^{3+} and Tb^{3+}) concentration was kept as low as reasonably achievable and the experiments were designed in such a way that the total doping concentration added up to ~2 mol%. For example, the typical concentrations of Ce and Tb ion pairs used were, respectively, 0.86 and 1.14 mol%, 1 and 1 mol% and 1.33 and 0.66 mol%.

2.2. Characterization

Room temperature X-ray diffraction (XRD) patterns were recorded from 10° to 75° (2θ) using a PANalytical X'Pert PRO diffractometer with wavelength radiation of 1.5406 Å (Cu Kα). Luminescent properties were investigated at room temperature using Hitachi F-7000 fluorescence spectrophotometer. The decay data were recorded using an inverted-type scanning confocal microscope (MicroTime-200, Picoquant, Germany). A single-mode pulsed diode laser (375 nm wavelength with an instrumental response function of ~240 ps in full-width at half maximum, 40 MHz repetition rate, and an average power ~1 μW) was used as an excitation source. The morphological and structural properties were investigated using FEI Tecnai-F20G2 high-resolution transmission electron microscopy (HRTEM) with an accelerating voltage of 200 kV. The chemical composition was analyzed using a PHI-5000 versaprobe X-ray photoelectron spectrometer (XPS). The XPS data were collected when the samples were irradiated with a monochromatic Al Kα radiation ($h\nu$ = 1486.6 eV). Survey scans were performed using a 1 eV/step (binding energies ranging from 0 to 1400 eV). The sample area analyzed was about 1 mm^2 and the pressure during data acquisition was typically under 1×10^{-8} Torr. The experimental curves were fitted using *Multipack v8.2c* data analysis software provided with the PHI-5000 versaprobe ESCA instrument that made use of a combination of Gaussian–Lorentzian peaks.

3. Results and discussion

3.1. XRD analysis

The XRD patterns of pure/undoped and Ce^{3+}–Tb^{2+} co-activated $ZnAl_2O_4$ are, respectively, shown in Figs. 1 and 2. Undoped $ZnAl_2O_4$ samples in Fig. 1 were (a) as prepared and (b) annealed in air at 600 °C and (c) 700 °C for 4 h, respectively. Fig. 2 shows the room temperature XRD patterns of the $ZnAl_2O_4$:Ce^{3+},Tb^{3+} samples annealed at 700 °C in a hydrogen atmosphere for 4 h. The concentrations of Ce^{3+} and Tb^{3+} were (a) 1.33 mol%, 0.66 mol%; (b) 1.14 mol%, 0.86 mol%; (c) 1 mol%, 1 mol%; (d) 0.66 mol%, 1.33 mol%; and (e) 0.86 mol%, 1.14 mol%. The diffraction patterns of Figs. 1 and 2 confirmed that all the samples consisted of $ZnAl_2O_4$ spinel structure with space group *Fd*3*m* as indexed by JCPDS file no. 01-082-1043. All the peaks obtained are in agreement with the spinel structure reported by Zawadzki et al. [25]. The intensity of the peaks relative to the background signal demonstrates high crystallinity of the samples. The peak intensities and the FWHM values (not shown) of undoped $ZnAl_2O_4$ phosphors in Fig. 1 were approximately the same regardless of annealing. It therefore shows that even without post-preparation annealing, highly crystalline material can be obtained at a processing temperature as low as 400 °C. This result is different from conventional solid state reaction where high processing temperature (usually >400 °C) is required to enhance crystallinity. Although the XRD patterns of Fig. 2 resemble those of Fig. 1, the peaks have broadened and their intensities were also reduced. It is well known that in addition to instrumental setup, the diffraction peak broadening is also a result of the crystallite sizes and lattice strains i.e. large crystallite sizes cause sharp reflections whereas small sizes lead to broad reflections, and variations in lattice spacings due to lattice strains can also cause broadening [26]. Since the same procedure was used to prepare all samples in this study, the crystallite size of the samples with or without activators (Ce^{3+} and Tb^{3+}) are expected to be in the same range. The peak broadening of Fig. 2 is therefore attributed to lattice strains due to incorporation of the Ce^{3+} and Tb^{3+} activator ions. Note that Ce^{3+} and Tb^{3+}

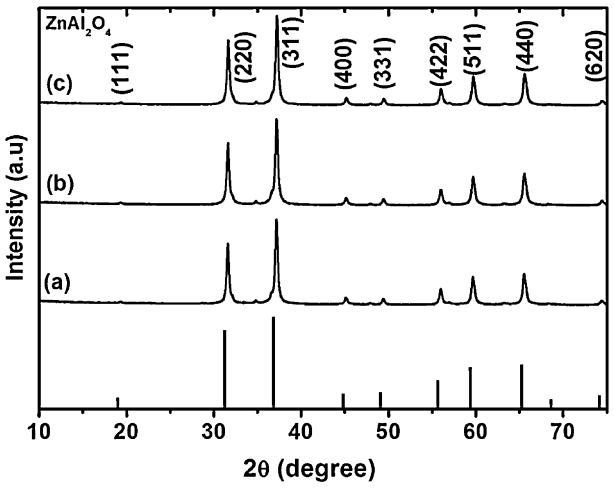

Fig. 1. Room temperature XRD patterns of $ZnAl_2O_4$ (a), as-prepared (b), annealed at 600 °C (c) and 700 °C in air for 4 h.

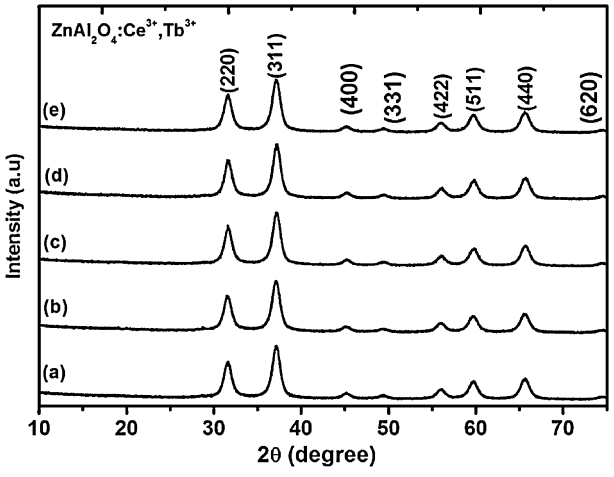

Fig. 2. Room temperature XRD patterns of annealed $ZnAl_2O_4$:Ce^{3+},Tb^{3+} with different concentrations of Ce^{3+} and Tb^{3+}.

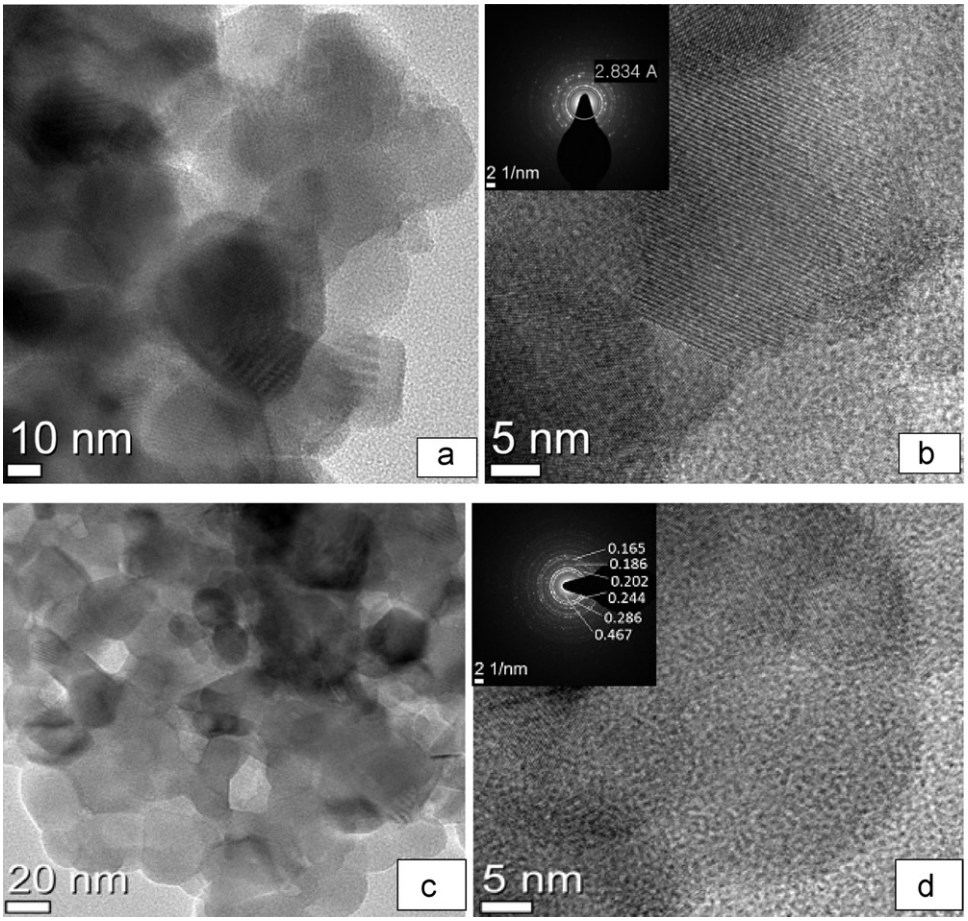

Fig. 3. (a) TEM image of $ZnAl_2O_4$:0.86 mol% Ce^{3+} –1.14 mol% Tb^{3+} showing agglomerated particles and (b) an enlarged view of the same sample showing fringes corresponding to the atomic planes. The inset is the selected area diffraction patterns of the same sample.

are expected to occupy Al^{3+} sites in the $ZnAl_2O_4$ lattice and since the ionic radii of Ce^{3+} (1.11 Å) and Tb^{3+} (1.00 Å) are larger than that of Al^{3+} (0.50 Å), their incorporation will most likely strain the lattice. The unidentified XRD peak at 34.6° may be attributed to species/impurities such as aluminum oxides, hydroxides and oxy-hydroxides in the tetrahedral environment.

3.2. TEM analysis

Transmission electron microscope (TEM) images of pure $ZnAl_2O_4$ and $ZnAl_2O_4$:Ce^{3+},Tb^{3+} powder annealed in a hydrogen atmosphere are shown in Fig. 3. The concentrations of Ce^{3+} and Tb^{3+} were 0.86 and 1.14 mol%, respectively. Fig. 3(a) and (c) shows agglomerated $ZnAl_2O_4$ and $ZnAl_2O_4$:Ce^{3+},Tb^{3+} particles with individual particle appearing circular (implying spherical shapes, although some faceting exists) with an average diameter of ~20 nm. HRTEM image in Fig. 3(b and d) shows well defined lattice fringes in various regions with agglomerated particles. As shown by lattice fringes in the images (Fig. 3(b) and (d)), this sample is highly crystalline and is consistent with the XRD data. The lattice spacing estimated from the selected area diffraction pattern (inset – Fig. 3(d)) was 0.24 nm, corresponding to the (3 1 1) lattice spacing of $ZnAl_2O_4$ [27].

3.3. Photoluminescence

Photoluminescence emission spectra of $ZnAl_2O_4$:Ce^{3+},Tb^{3+} nano-powder phosphors and that of Ce^{3+} (2 mol%) singly doped $ZnAl_2O_4$ are presented in Fig. 4. The $ZnAl_2O_4$:Ce^{3+},Tb^{3+} nanopowders with different concentrations of Ce^{3+} and Tb^{3+} were excited in air at room temperature using different excitation wavelengths. The emission spectrum of Ce^{3+} singly doped $ZnAl_2O_4$ phosphor excited at 256 nm consists of a broad band with two maxima at 350 and 410 nm. These emissions correspond to the allowed transitions from the lowest sublevel of the 5d state to the $^2F_{7/2}$ and $^2F_{5/2}$ multiplets of the 4f configuration of Ce^{3+} [28]. Dual

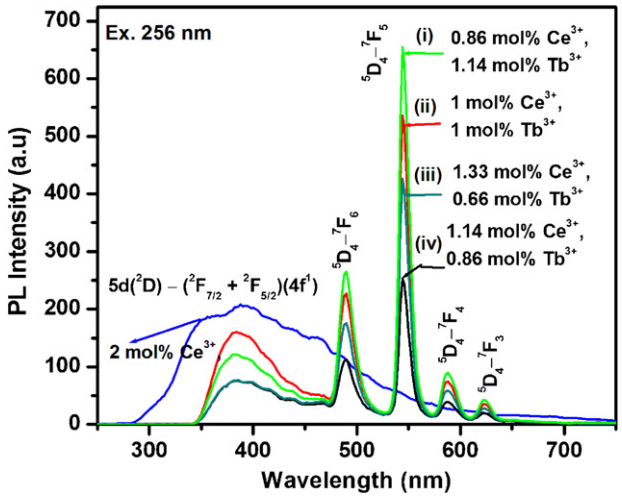

Fig. 4. PL emission spectra of annealed $ZnAl_2O_4$:Ce^{3+},Tb^{3+} with different concentrations of Ce^{3+} and Tb^{3+}.

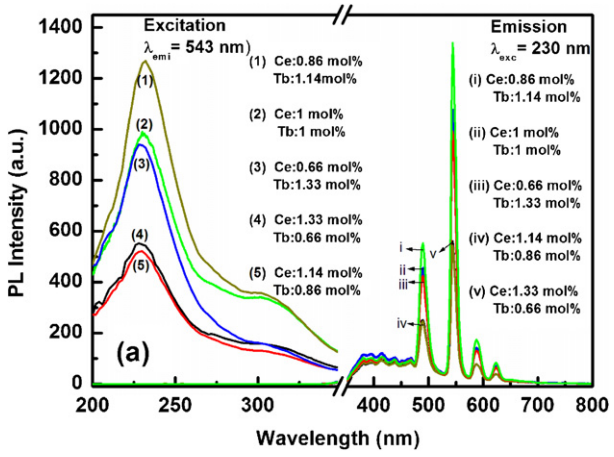

Fig. 5. PL and PLE spectra of $ZnAl_2O_4$:Ce^{3+},Tb^{3+} excited at 230 nm.

emission was observed from the $ZnAl_2O_4$ powders co-activated with different concentrations of Ce^{3+} and Tb^{3+}. This was a combination of line emissions from Tb^{3+} ions and broad emission from Ce^{3+}. The green line emission associated with $^5D_4 \rightarrow {}^7F_5$ transitions of Tb^{3+} at 544 nm was more intense than the purplish-blue broad emission of Ce^{3+} at 350–410 nm. The green emission was maximized when 1.14 mol% of Tb^{3+} was co-doped with 0.86 mol% of Ce^{3+}. The enhancement of the green emission and the subsequent decrease in the blue emission suggests that energy was transferred, most probably by phonon mediated processes, from Ce^{3+} to Tb^{3+}. This transfer of energy is a well established phenomenon found in several host matrices. For example, energy transfer from Ce^{3+} to Tb^{3+} was demonstrated in amorphous SiO_2 host [29]. It is demonstrated in this study that in addition to energy transfer through direct excitation of Ce^{3+}, the emission intensity is also dependent on the excitation wavelength. For example, from the list of selected excitation wavelengths (230–325 nm), the most intense excitation was observed at 230 nm and it gave green emission (λ_{em} = 544 nm) in all the samples. The excitation at 230 nm is consistent with the 232 nm excitation attributed to the $4f^8 \rightarrow 4f^85d^1$ transitions of Tb^{3+} by Barros et al. [11].

Fig. 5 shows the PL excitation (λ_{em} = 544 nm) and emission (λ_{exc} = 230 nm) of $ZnAl_2O_4$ powders with different concentrations of Ce^{3+} and Tb^{3+}. The most intense green emission was observed from the powder co-doped with 1.14 mol% of Tb^{3+} and 0.86 mol% of Ce^{3+}. The maximum intensity as a function of excitation wavelength of 1.14 mol% of Tb^{3+} and 0.86 mol% of Ce^{3+} co-doping shown in Fig. 6 confirms that the 230 nm excitation gave the most intense green emission at λ_{em} = 544 nm. The other excitation wavelengths (256, 300 and 325 nm) with relatively less intense emissions can be attributed to either direct excitation of Ce^{3+} or charge transfer transition from O^{2-} to Tb^{3+}.

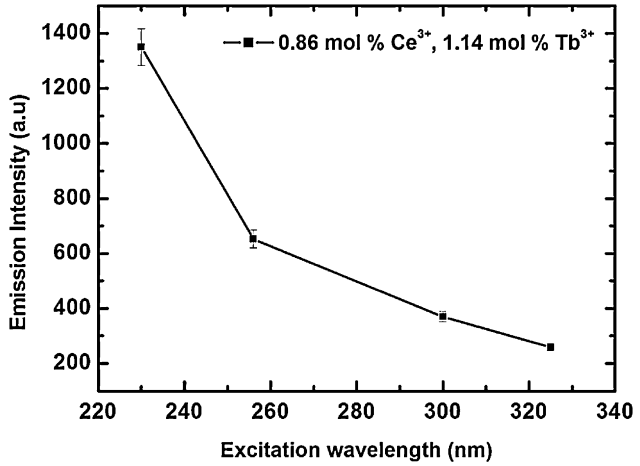

Fig. 6. Maximum emission intensity of $ZnAl_2O_4$:0.86 mol% Ce^{3+}, 1.14 mol% Tb^{3+} (λ_{em} = 544 nm) as a function of excitation wavelengths (230, 256, 300 and 325 nm).

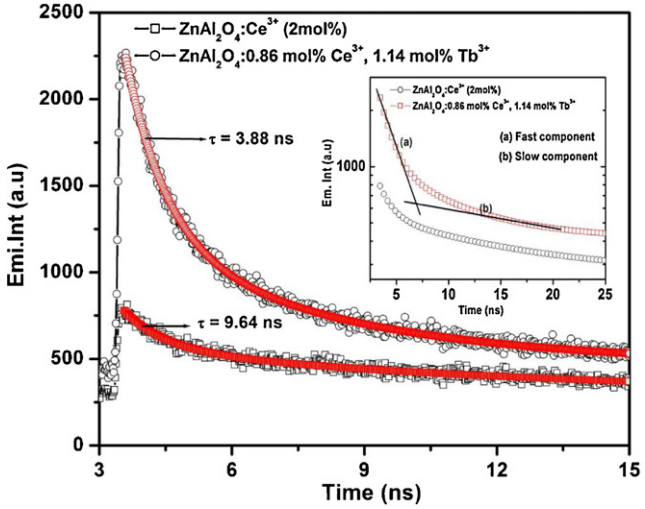

Fig. 7. Decay curves of the $ZnAl_2O_4$:Ce^{3+} (2 mol%) and $ZnAl_2O_4$:0.86 mol% Ce^{3+}, 1.14 mol% Tb^{3+} measured in air at room temperature. The solid (red) lines are the fitted curves. (For interpretation of the references to color in this figure legend, the reader is referred to the web version of the article.)

3.4. Decay dynamics of Ce^{3+} singly doped and Ce^{3+}–Tb^{3+} co-doped $ZnAl_2O_4$

Fig. 7 compares the fluorescence decay dynamics of singly activated and $ZnAl_2O_4$:Ce^{3+} (2 mol%) and $ZnAl_2O_4$:Ce^{3+},Tb^{3+} (0.86 mol%, 1.14 mol%) powders, which gave the maximum PL intensity. The powders were excited at 375 nm monitoring Ce^{3+} emission at 410 nm. A single-mode pulsed diode laser wavelength with an instrumental reponse function of ~240 ps in full-width at half maximum, 40 MHz repetition rate, and an average power of ~1 μW was used. The decay curves were fitted using the bi-exponential function:

$$I = A_1 \exp\left(\frac{-t_1}{\tau_1}\right) + A_2 \exp\left(\frac{-t_2}{\tau_2}\right), \quad (1)$$

where I represents the phosphorescent intensity; A_1 and A_2 are constants; t_1 and t_2 are the decay times and τ_1 and τ_2 are the decay constants. The fitting parameters are presented in Table 1. The average lifetimes were calculated using the following equation:

$$(\tau) = \frac{A_1\tau_1^2 + A_2\tau_2^2}{A_1\tau_1 + A_2\tau_2} \quad (2)$$

The lifetime values for the Ce^{3+} singly activated and Ce^{3+}–Tb^{3+} co-activated $ZnAl_2O_4$ samples were 9.62 and 3.88 ns, respectively. The fact that the average lifetime of the Ce^{3+}–Tb^{3+} co-activated sample was shorter than the Ce^{3+} singly activated sample indicates that the decay rate of the 410 nm emission was faster in the co-

Table 1
Fitting parameters for the half life times of $ZnAl_2O_4$:Ce^{3+} and $ZnAl_2O_4$:Ce^{3+},Tb^{3+}.

Sample name	Fitting parameters			
	A_1	τ_1 (ns)	A_2	τ_2 (ns)
$ZnAl_2O_4$:Ce^{3+}	225.54	0.968	275.22	10.31
$ZnAl_2O_4$:Ce^{3+},Tb^{3+}	1101.34	0.911	736.15	4.736

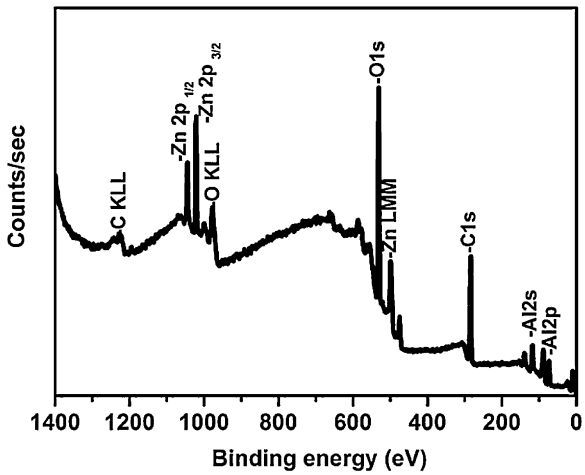

Fig. 8. X-ray photoelectron spectroscopy (XPS) survey scan of $ZnAl_2O_4$:Ce^{3+},Tb^{3+} phosphor.

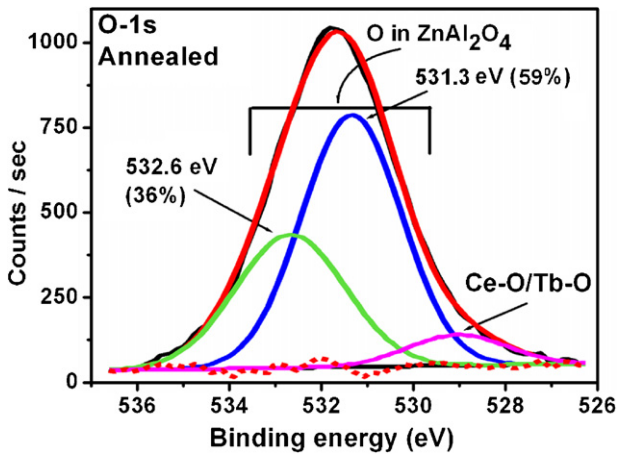

Fig. 10. XPS peak fitting of the O 1s peak after annealing $ZnAl_2O_4$:0.86% Ce^{3+}, 1.14% Tb^{3+} in hydrogen atmosphere.

activated sample. Since the decrease in the peak intensity of the 410 nm emission was simultaneous with the increase in the peak intensity of Tb^{3+} emission at 544 nm, it is reasonable to attribute the shorter life time (faster decay rate) of this emission to energy transfer from Ce^{3+} to Tb^{3+}. The simultaneous radiative emission and energy transfer from Ce^{3+} to Tb^{3+} suggests that Ce^{3+} is capable of creating a potential well for trapping charge carriers thereby playing a dual role of a luminescent and trap centre [30,31]. The inset of Fig. 7 shows that the bi-exponential decay curves can be resolved into two components, namely the fast and slow components with decay times of 0.911 ns and 4.736 ns, respectively. Birowosuto et al. [30] attributed the slow and fast components to exciton trapping by Ce^{3+} and lattice (and subsequent transfer to Ce^{3+}), respectively. The fitting parameters for $ZnAl_2O_4$:Ce^{3+} (2 mol%) and $ZnAl_2O_4$:0.86 mol% Ce^{3+}, 1.14 mol% Tb^{3+} samples are listed in Table 1.

3.5. X-ray photoelectron spectroscopy (XPS)

The chemical composition and electronic state of the $ZnAl_2O_4$:Ce^{3+},Tb^{3+} system were analyzed by XPS. The XPS survey spectrum in Fig. 8 confirms the presence of Al 2p, O 1s, Zn $2p_{3/2}$ and C 1s (from adventitious hydrocarbons) with binding energies (BE) of 74.2 eV, 531.1 eV, 1022.1 eV and 285.3 eV, respectively, on the surface. These values are consitent with those reported by Strohmeier [32].

Figs. 9 and 10 show, respectively, the fitted data for the O 1s peak from $ZnAl_2O_4$:0.86 mol% Ce^{3+}, 1.14 mol% Tb^{3+} powder before and after annealing. In both figures, the lattice O 1s peak was stable at ~531.1 eV suggesting that the chemical and hence electronic states were not affected by annealing in hydrogen. This peak is consistent with the O 1s peak with the binding energy of 531.4 eV reported by Strohmeier [32]. The satellite peaks at ~528.5 eV and ~529.5 eV in Figs. 9 and 10 can be assigned to binding energies of O 1s peak in Ce–O and Tb–O metallic oxides, respectively [33]. That is, it is most likely that small traces of CeO_x and TbO_x ($x \leq 2$) were present in both annealed and unannealed $ZnAl_2O_4$:Ce^{3+},Tb^{3+} samples. It is worth noting that these peaks were really small and in the noise levels of our measurements. Fig. 11 shows the XPS fittings of the O 1s peak from the sample annealed in hydrogen atmosphere. As in Fig. 10, the photoelectron peak position measured at 531.1 eV is consistent with the theoretical value of O 1s peak in $ZnAl_2O_4$ listed in ref. [32]. In addition, a new band appeared at 532.6 eV and it can be assigned to chemisorbed water and/or oxygen molecules from environmental moisture [34].

The fitted data of the Al 2p peak of the $ZnAl_2O_4$:0.86 mol% Ce^{3+}, 1.14 mol% Tb^{3+} before and after annealing are shown in Figs. 11 and 12, respectively. In both figures, the Al 2p peaks at lower binding energies (74.2 eV) can be assigned to Al ions occupying the tetrahedral (IV) sites while the Al 2p peaks at higher binding

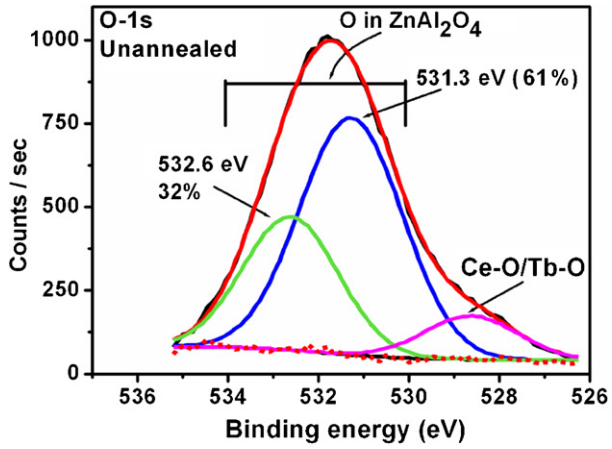

Fig. 9. XPS peak fitting of the O 1s peak from as-prepared $ZnAl_2O_4$:0.86% Ce^{3+}, 1.14% Tb^{3+}.

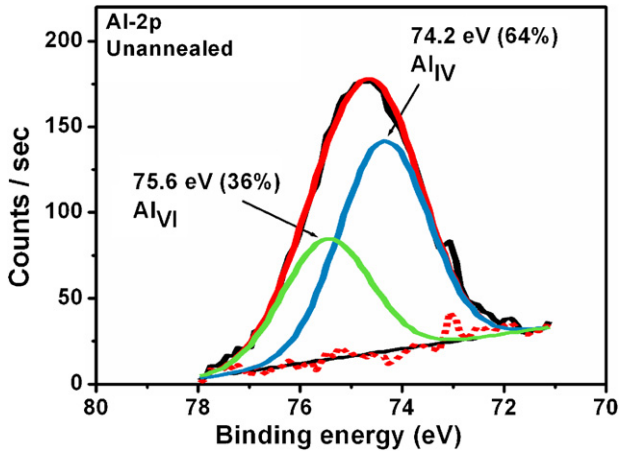

Fig. 11. XPS peak fitting of the Al 2p peak from as-prepared $ZnAl_2O_4$:0.86% Ce^{3+}, 1.14% Tb^{3+}.

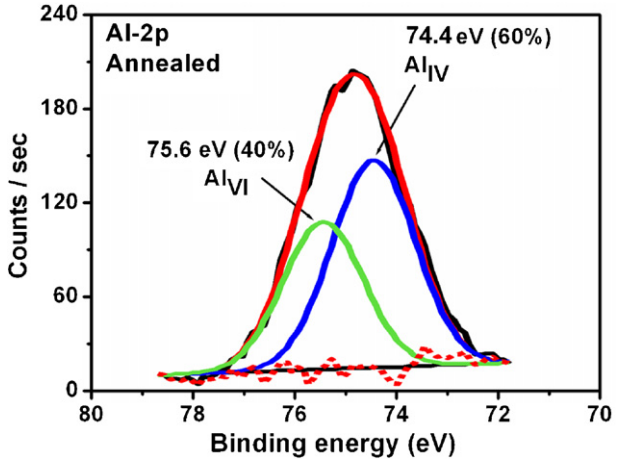

Fig. 12. XPS peak fitting of the Al 2p peak from as-prepared $ZnAl_2O_4$:0.86% Ce^{3+}, 1.14% Tb^{3+}.

energies (75.6 eV) can be assigned to the Al ions occupying the octahedral (VI) sites. This assignment is consistent with the Al 2p peak analysis for yttrium aluminum garnet, $Y_3Al_5O_{12}$ (YAG), reported by Pawlak et al. [35]. Furthermore, they reported the peak area ratio of the Al 2p in the octahedral to tetrahedral sites of 2:3 (40%:60%).

Note that it is generally accepted that when a material consists of a mixture of octahedral and tetrahedral bonded oxides, the octahedral site is more cationic with a partial positive charge ($\delta+$) and the tetrahedral site will be more anionic with a partial negative charge ($\delta-$) [35]. It is therefore reasonable to assign the tetrahedral site to less binding energy because less energy is required to remove an electron from a more anionic species. The concentrations of Al in the octahedral and tetrahedral sites of the unannealed sample (Fig. 11) as determined from the area of the fitted Al peaks were 36% and 64%, respectively. Recall that the high concentration of 3+ ions (Al^{3+}) in the tetrahedral site with respect to that in the octahedral site points to the partial inversion of the $ZnAl_2O_4$ nanocrystal structure. Upon annealing, the concentration of Al in the octahedral site increased from 36% to 40%, while that in the tetrahedral site decreased from 64% to 60% as shown in Fig. 12. This can be attributed to possible structural readjustment from inverse to normal spinel as a result of annealing. In the spinel structure it is physically impossible for more than 50% of the trivalent ions to occupy tetrahedral sites as implied in this case. It must, however, be pointed out that XPS is a surface sensitive technique, with the XPS signal coming from the top few layers which might be slightly different from the bulk. Extra contributions from possible surface species/impurities such as aluminum oxides, hydroxides and oxyhydroxides with binding energies around 73.7 eV might contribute toward the excess amount of Al in the tetrahedral sites.

4. Conclusions

In conclusion, the $ZnAl_2O_4$:Ce^{3+},Tb^{3+} powder phosphors were successfully synthesized using a one-step combustion technique. As confirmed from the X-ray diffraction data, the $ZnAl_2O_4$ was highly crystalline with or without post-synthesis annealing. The X-ray photoelectron spectroscopy data confirmed that there was structural readjustment from inverse to normal spinel as a result of annealing. The TEM data showed that the particles were spherical in shape, with some degree of faceting, and their average size was ~20 nm in diameter. The PL intensity of the green line emission from Tb^{3+} at 544 nm increased as a result of Ce^{3+} co-doping. The fact that the increase was simultaneous with the decrease in blue emission from Ce^{3+} suggests that excitation energy was transferred from Ce^{3+} to Tb^{3+}. The maximum intensity was obtained from the sample co-activated with 0.86 mol% of Ce^{3+} and 1.14 mol% of Tb^{3+} when the sample was excited at 230 nm. The other excitation wavelengths (256, 300 and 325 nm) with relatively less intense emissions were attributed to either direct excitation of Ce^{3+} or charge transfer transition from O^{2-} to Tb^{3+}. It therefore shows that the activator concentration and excitation wavelength are important parameters for sensitized emission of phosphors by the UV down-conversion process.

Acknowledgements

The authors would like to thank the South African National Research Foundation (NRF), National Research Foundation of Korea and Nanomaterials Cluster fund of the University of the Free State for the financial support. Authors also give special thanks to Dr. Weon-Sik Chae, Korea Basic Science Institute, for the fluorescence lifetime measurement.

References

[1] Z. Lou, J. Hao, Appl. Phys. A 80 (2005) 151–154.
[2] S. Mathur, M. Veith, M. Haas, H. Shen, N. Lecerf, V. Huch, S. Hufner, R. Haberkon, H.P. Beck, M. Jilavi, J. Am. Ceram. Soc. 84 (9) (2001) 1921–1928.
[3] R.F. Martinez, O.A. Serra, J. Braz. Chem. Soc. 21 (7) (2010) 1395–1398.
[4] V. Ciupina, I. Garazeanu, G. Prodan, J. Opt. Adv. Mater. 6 (4) (2004) 1317–1322.
[5] X. Wang, M. Zhang, H. Ding, H. Li, Z. Sun, J. Alloys Compd. 509 (2011) 6317–6320.
[6] F. Davar, M. Salvati-Niasari, J. Alloys Compd. 509 (2011) 2481–2492.
[7] J. Popović, B. Gržeta, B. Rakvin, E. Tkalčec, M. Vrankić, S. Kuranjica, J. Alloys Compd. 509 (2011) 8487–8492.
[8] J. Zhao, H. Chai, F. Zhang, JMEPEG 19 (2010) 46–51.
[9] X. Duan, D. Yuan, X. Wang, H. Xu, J. Sol–Gel Sci. Technol. 35 (2005) 221–224.
[10] M. Zawadzki, J. Wrzdyszcz, W. Strek, D. Hreniak, J. Alloys Compd. 332–324 (2001) 279–282.
[11] B.S. Barros, P.S. Mellow, R.H.G.A. Kiminami, A.C.F.M. Costa, G.F. de Sá, S. Alves Jr., J. Mater. Sci. 41 (2006) 4744–4748.
[12] S.F. Wang, F. Gu, M.K. Lu, X.F. Cheng, W.G. Zhou, G.J. Zhou, S.M. Wang, Y.Y. Zhou, J. Alloys Compd. 394 (2005) 255–258.
[13] I. Mindru, G. Marinescu, D. Gingasu, L. Patron, L. Diamandescu, C. Ghica, B. Mironov, Mater. Sci. Eng. B 170 (2010) 99–106.
[14] H.H. Le, T.L. Phung, N.L. Nguyen, T.L. Trinh, J. Phys: Conf. Ser. 187 (2009) 012053 (1–6).
[15] S.S. Pitale, V. Kumar, I.M. Nagpure, O.M. Ntwaeaborwa, H.C. Swart, Appl. Surf. Sci. 257 (2011) 3298–3306.
[16] Y. Wu, J. Du, K.-L. Choy, L.L. Hench, J. Guo, Thin Solid Films 472 (1–2) (2005) 150–156.
[17] M.-T. Tsai, Y.-X. Chen, P.-J. Tsai, Y.-K. Wang, Thin Solid Films 518 (24) (2010) e9–e11.
[18] C.-C. Yang, S.-Y. Chen, S.-Y. Cheng, Powder Technol. 148 (1) (2004) 3–6.
[19] X.Y. Chen, C. Ma, Opt. Mater. 32 (2010) 415–421.
[20] V. Singh, V. Natarajan, J.-J. Zhu, Opt. Mater. 29 (2007) 1447–1451.
[21] N.J. van der Laag, M.D. Snel, P.C.M.M. Magusin, G. de With, J. Eur. Ceram. Soc. 24 (8) (2004) 2417–2424.
[22] T. Mimani, J. Alloys Compd. 315 (2001) 123.
[23] P. Thiyagarajan, M. Kottaisamy, M.S. Ramachandra Rao, J. Lumin. 129 (9) (2009) 991–995.
[24] Q.Y. Zhang, X.Y. Huang, Prog. Mater. Sci. 55 (5) (2010) 353–427.
[25] M. Zawadzki, W. Staszak, F.E. López-Suárez, M.J. Illán-Gómez, A. Bueno-López, Appl. Catal. A: Gen. 371 (1-2) (2009) 92–98.
[26] J.-D. Kaminga, L.J. Seijbel, J. Res. Inst. Stand. Technol. 109 (2004) 64–75.
[27] A.A. da Silva, A.S. Goncalves, M.R. Davolos, S.H. Santagneli, J. Nanosci. Nanotechnol. 8 (2008) 5691.
[28] V.R. Bandi, Y.T. Nien, I.G. Chen, J. Appl. Phys. 108 (2010), 02311-2.
[29] O.M. Ntwaeaborwa, H.C. Swart, R.E. Kroon, P.H. Holloway, J.R. Botha, J. Phys. Chem. Solids 67 (2006) 1749–1753.
[30] M.D. Birowosuto, P. Dorenbos, C.W.E. van Eijk, K.W. Krämer, H.U. Güdel, Phys. Status Solidi A 204 (3) (2007) 850–860.
[31] E.V.D. van Loef, P. Dorenbos, C.W.E. van Eijk, K.W. Krämer, H.U. Güdel, Nucl. Instrum. Methods Phys. Res. A 496 (2003) 138–145.
[32] B.R. Strohmeier, Surf. Sci. Spectra 3 (1995) 129–134.
[33] J.F. Moulder, W.F. Stickle, P.E. Sobol, K.D. Bomben, Handbook of X-ray Photoelectron Spectroscopy, Physical Electronic, Inc., Minnnesota, USA, 1995.
[34] S.J. Kerber, J.J. Bruckner, K. Wozniak, S. Seal, S. Hardcastle, T.L. Barr, J. Vac. Sci. Technol. A 14 (3) (1996) 1314–1320.
[35] D.A. Pawlak, K. Wozniak, Z. Frukacz, T.L. Barr, D. Fiorentino, S. Seal, J. Phys. Chem. B 103 (1999) 1454–1461.